Aspects of chiral symmetry in QCD at $T = 128$ MeV

Marco Cè,[1] Tim Harris,[2] Ardit Krasniqi,[3,*] Harvey B. Meyer,[3,4,5] and Csaba Török[3]

[1]*Albert Einstein Center for Fundamental Physics (AEC) and Institut für Theoretische Physik,
Universität Bern, Sidlerstrasse 5, CH-3012 Bern, Switzerland*
[2]*School of Physics and Astronomy, University of Edinburgh, Edinburgh EH9 3JZ, United Kingdom*
[3]*PRISMA+ Cluster of Excellence and Institut für Kernphysik, Johannes Gutenberg-Universität Mainz,
D-55099 Mainz, Germany*
[4]*Helmholtz Institut Mainz, Johannes Gutenberg-Universität Mainz, D-55099 Mainz, Germany*
[5]*GSI Helmholtzzentrum für Schwerionenforschung, 64291 Darmstadt, Germany*

We investigate several aspects of chiral symmetry in QCD at a temperature of $T = 128$ MeV. The study is based on a 24×96^3 lattice-QCD ensemble with O(a)-improved Wilson quarks and physical up, down and strange quark masses. The pion quasiparticle turns out to be significantly lighter than the zero-temperature pion mass, even though the corresponding static correlation length is shorter. We perform a quantitative comparison of our findings to predictions of chiral perturbation theory. Among several order parameters for chiral symmetry restoration, we compute the difference of the vector- and axial-vector time-dependent correlators and find it to be reduced by a factor $\sim 2/3$ as compared to its vacuum counterpart.

I. INTRODUCTION

Quark matter under extreme conditions (high temperatures and densities) is interesting both from the experimental and theoretical point of view. In the early Universe [on a timescale of $\mathcal{O}(\mu s)$], the strongly interacting constituents (quarks and gluons) were in a hot and dense phase called quark-gluon plasma (QGP). Heavy ion colliders enable similar conditions to be reached in the lab. As a result of its expansion, the universe gradually cooled down, undergoing a phase transition to a hadronic phase in which we now find ourselves. Note that at physical quark masses the transition is actually a crossover characterized by a pseudocritical temperature $T_{pc} = 156.5(1.5)$ MeV [1]. In the limit of massless quarks, the QCD Lagrangian has a global symmetry in flavor space, $SU(N_f)_L \times SU(N_f)_R$, corresponding to two independent rotations of the left- and right-handed components of the Dirac fields. This symmetry is spontaneously broken to $SU(N_f)_V$ and should be restored in the high-temperature phase (chiral symmetry restoration). A nonvanishing value of the scalar density $\langle \bar{\psi}\psi \rangle(T)$ characterizes the low-temperature phase

*Corresponding author.
arkrasni@uni-mainz.de

$(0 \leq T \leq T_c \approx 132$ MeV [2]). On the contrary, $\langle \bar{\psi}\psi \rangle(T) = 0$ for $T > T_c$, indicating that chiral symmetry is restored. Thus, the quark condensate $\langle \bar{\psi}\psi \rangle$ is a true order parameter for chiral symmetry breaking. A direct consequence of a restored chiral symmetry would be a coincidence of vector and axial-vector spectral function (see Sec. V C).

Starting in the QCD vacuum, increasing the temperature initially leads to a dilute gas of pions. As the temperature is further increased, other hadron species also begin to contribute. At the same time, one expects the excitations of the medium to be quasiparticles with somewhat modified properties as compared to the standard hadrons, which are excitations of the vacuum. A natural starting point in the investigation of the medium's quasiparticles is to examine the properties of the pion in the thermal environment [3,4]. The pion mass and the pion decay constant have been studied to one loop in a thermal chiral perturbation theory (ChPT) approach [5]. Additionally, the energy density, the pressure and the quark condensate have been investigated up to $\mathcal{O}(p^8)$ in a chiral expansion below the phase transition [6]. In Ref. [7] the shift in the pion pole was calculated as a function of temperature up to second order in the density. Toublan [8] calculated also the pion decay constant within thermal ChPT to two loops and additionally examined the validity of the Gell-Mann-Oakes-Renner (GOR) relation at finite temperature. Unfortunately, it is unclear how far up in the temperature this expansion is applicable, since the partition function is certainly no longer dominated by the pions for $T \gtrsim 100$ MeV [3,6]. However, the Goldstone-boson nature of pions guarantees

the existence of a divergent static correlation length for vanishing quark masses [9].

In standard thermal ChPT, the quark mass as well as the temperature are treated as small parameters, resulting in an expansion around $m_q = 0$ and $T = 0$. In Refs. [10,11], however, Son and Stephanov investigated perturbations only around $m_q = 0$, keeping the temperature T fixed to any value in the chirally broken phase. Although an explicit relation of parameters like the quark condensate and pion decay constant to their $T = 0$ counterparts is no longer possible in this framework, the validity of their results is extended to a regime where neither ChPT nor perturbative QCD is usable. Since lattice simulations rely on the imaginary-time formalism and due to the lack of Lorentz invariance at finite temperature, extracting real-time observables such as "pole masses" out of lattice quantities (e.g. Euclidean correlators) is a nontrivial task. Nevertheless, within the chiral effective theory approach of Son and Stephanov, the real part of the dispersion relation of soft pions can be obtained in terms of static Euclidean correlators. For the $N_f = 2$ case this has been done in Refs. [12,13].

The paper is structured as follows: In Sec. II we start with the introduction of some basic definitions which have a key role in the description of the pion quasiparticle. We continue with the implementation of the lattice correlators, followed by a brief description of the numerical setup. Our results, divided into subsections, are presented in Sec. III. First we extract the mass and decay constant of the screening pion (Secs. III A and III B). Next, we determine the pion velocity u and examine its dependence on a finite pion thermal width $\Gamma(T)$ (Secs. III C and III D). Subsequently, we reconstruct a smeared and rescaled version of the axial spectral function and compare our results with the literature (Secs. III E and III F). Thereafter, we compare our lattice estimate for the quark number susceptibility with the prediction from the hadron resonance gas model (HRG) in Sec. IV. We also investigate in that section the effect of a modified dispersion relation for the pion in the HRG. Finally, we look at several order parameters for chiral symmetry restoration in Sec. V and give our conclusions in Sec. VI.

II. PRELIMINARIES

In this section we introduce the notation and some basic definitions as well as the key quantities for the pion quasiparticle that we will use throughout the paper. Furthermore, the lattice implementation of the correlators and the numerical setup are described briefly.

A. Definition of operators and correlation functions

The notation and conventions used in this work are adapted from Ref. [12]. Our framework is the light-quark sector of Euclideanized QCD on the space $S^1 \times \mathbb{R}^3$, S^1 denoting the Matsubara cycle of length $\beta \equiv 1/T$. We de-

fine the pseudoscalar density, the vector current and the axial-vector current as

$$P^a(x) = \bar{\psi}(x)\gamma_5 \frac{\tau^a}{2}\psi(x), \qquad V^a_\mu(x) = \bar{\psi}(x)\gamma_\mu \frac{\tau^a}{2}\psi(x),$$

$$A^a_\mu(x) = \bar{\psi}(x)\gamma_\mu\gamma_5 \frac{\tau^a}{2}\psi(x), \tag{1}$$

where $a \in \{1, 2, 3\}$ is an adjoint $SU(2)_{\text{isospin}}$ index, τ^a is a Pauli matrix and $\psi(x)$ is a Dirac field flavor doublet. The partially conserved axial current (PCAC) relation is an operator identity that holds in Euclidean space when inserted in expectation values. It relates the divergence of the axial vector current $A^a_\mu(x)$ to the pseudoscalar density $P^a(x)$,

$$\partial_\mu A^a_\mu(x) = 2m_{\text{PCAC}} P^a(x). \tag{2}$$

In the path integral formulation, this relation results from performing a chiral rotation $\delta^a_A \psi(x) = \frac{\tau^a}{2}\gamma_5 \psi(x)$ of the fields (see Ref. [14]). Applying the pseudoscalar density operator on both sides and taking the expectation value one can solve for the bare PCAC quark mass,

$$m_{\text{PCAC}} = \frac{1}{2}\frac{\partial_\mu \langle A^a_\mu(x) P^a(0)\rangle}{\langle P^b(x) P^b(0)\rangle}. \tag{3}$$

Since the PCAC relation is an operator identity, we are free to choose the direction in which we define the quark mass. In our thermal system, the spatial direction is four times larger than the temporal one. As a consequence, measuring along the spatial direction results in a longer plateau and thus, smaller errors. Therefore, we will extract the PCAC quark mass from the relation

$$m_{\text{PCAC}}(x_3) = \frac{1}{2}\frac{\int dx_0 d^2x_\perp \langle \tilde{\partial}_3 A^a_3(x) P^a(0)\rangle}{\int dx_0 d^2x_\perp \langle P^b(x) P^b(0)\rangle}, \quad x_\perp = (x_1, x_2). \tag{4}$$

We introduce the static screening axial correlator, given by

$$\delta^{ab} G^s_A(x_3, T)$$

$$= \int dx_0 d^2x_\perp \langle A^a_3(x) A^b_3(0)\rangle \overset{|x_3| \to \infty}{=} \delta^{ab}\frac{f^2_\pi m_\pi}{2}e^{-m_\pi|x_3|}, \tag{5}$$

where we have specified the asymptotic form of the correlator, which defines the screening pion mass m_π and decay constant f_π. Analogously, we define the following static screening correlators:

$$\delta^{ab} G^s_P(x_3, T) = \int dx_0 d^2x_\perp \langle P^a(x) P^b(0)\rangle, \tag{6}$$

$$\delta^{ab} G^s_{AP}(x_3, T) = \int dx_0 d^2x_\perp \langle A^a_3(x) P^b(0)\rangle. \tag{7}$$

The PCAC relation [see Eq. (2)] implies the relation

$$G_P^s(x_3, T) = -\frac{1}{4m_{\text{PCAC}}^2} \frac{\partial^2}{\partial x_3^2} G_A^s(x_3, T). \tag{8}$$

In order to probe the dynamical properties of the thermal system, we define time-dependent correlators, projected to a definite spatial momentum,

$$\delta^{ab} G_{A_0}(x_0, T) = \int d^3 x \langle A_0^a(x) A_0^b(0) \rangle, \tag{9}$$

$$\delta^{ab} G_P(x_0, T) = \int d^3 x \langle P^a(x) P^b(0) \rangle, \tag{10}$$

$$\delta^{ab} G_{PA_0}(x_0, T) = \int d^3 x \langle P^a(x) A_0^b(0) \rangle$$
$$= -\int d^3 x \langle A_0^a(x) P^b(0) \rangle, \tag{11}$$

$$\delta^{ab} G_A(x_0, \mathbf{p}, T) = -\frac{1}{3} \sum_{i=1}^{3} \int d^3 x \, e^{-i\mathbf{p} \cdot \mathbf{x}} \langle A_i^a(x) A_i^b(0) \rangle, \tag{12}$$

$$\delta^{ab} G_V(x_0, \mathbf{p}, T) = -\frac{1}{3} \sum_{i=1}^{3} \int d^3 x \, e^{-i\mathbf{p} \cdot \mathbf{x}} \langle V_i^a(x) V_i^b(0) \rangle. \tag{13}$$

The time-dependent axial correlator $G_A(x_0, T)$ [see Eq. (12)] can be obtained from the spectral function $\rho_A(\omega, T, \mathbf{p})$ (see e.g. the review [15]):

$$G_A(x_0, T, \mathbf{p}) = \int_0^\infty d\omega \, \rho_A(\omega, \mathbf{p}, T) \frac{\cosh(\omega(\beta/2 - x_0))}{\sinh(\omega\beta/2)}. \tag{14}$$

In Sec. III E we will analyze the axial spectral function using the Backus-Gilbert method. Relations analogous to Eq. (14) hold for the correlators $G_{A_0}(x_0, T)$, $G_P(x_0, T)$ and $G_V(x_0, \mathbf{p}, T)$.

B. Pion properties at finite temperature

It has been established within several frameworks [10,11] that at temperatures well below the chiral phase transition a pion quasiparticle persists, with the real part of the dispersion relation of sufficiently soft pions given by

$$\omega_{\mathbf{p}} = u(T)\sqrt{m_\pi^2 + \mathbf{p}^2}, \quad \text{for any } T \lesssim T_c. \tag{15}$$

In the chiral limit it can be interpreted as the group velocity of a massless pion excitation. While the quasiparticle mass $\omega_{\mathbf{0}}$ is the real-part of a pole of the retarded correlator $G_P^R(\omega, \mathbf{p} = 0, T)$ of the pseudoscalar density in the frequency variable, the screening mass m_π is a pole of

$G_P^R(\omega = 0, \mathbf{p}, T)$ in the spatial momentum $|\mathbf{p}|$ and represents an inverse spatial correlation length. A simple interpretation of the dispersion relation (15) was given in Ref. [13] in terms of the poles of the screening and the time-dependent correlators. Son and Stephanov [10,11] showed that the pion velocity u in the chiral limit is the ratio of two static quantities,

$$u^2 = \frac{f_\pi^2}{\int_0^\beta dx_0 G_{A_0}(x_0, T)}. \tag{16}$$

As noted in Ref. [12], the axial susceptibility appearing in the denominator of Eq. (16) contains an ultraviolet divergence at any nonvanishing quark mass and is therefore not practical for lattice calculations. As an alternative, in Refs. [12,13] the parameter u was determined using lattice correlation functions at vanishing spatial momentum via the two estimators,

$$u_m = \left[-\frac{4m_q^2}{m_\pi^2} \frac{G_P(x_0, T)}{G_{A_0}(x_0, T)} \Big|_{x_0 = \beta/2} \right]^{1/2}, \tag{17}$$

$$u_f = \frac{f_\pi^2 m_\pi}{2 G_{A_0}(\beta/2, T) \sinh(u_f m_\pi \beta/2)}, \tag{18}$$

which we will adopt. In doing so, for the estimator u_m, the parametric dominance of the pion in the time-dependent Euclidean axial as well as the pseudoscalar density correlator at small quark masses is exploited. The estimator u_f exploits only the parametric dominance of the axial correlator; on the other hand, it relies on the residue determined from the static screening correlator. The pion contribution to the spectral function ρ_{A_0} is expected to take the form of a sharp peak,

$$\rho_{A_0}(\omega, T) = \text{sgn}(\omega)\text{Res}(\omega_{\mathbf{0}})\delta(\omega^2 - \omega_{\mathbf{0}}^2) + \ldots, \tag{19}$$

where in Ref. [11] (see also Ref. [13]) the residue was predicted to have the form

$$\text{Res}(\omega_{\mathbf{0}}) \equiv (f_\pi^t)^2 \omega_0^2 = f_\pi^2 m_\pi^2, \tag{20}$$

such that we can access the quasiparticle decay constant via $f_\pi^t = f_\pi/u_m$.

C. Lattice implementation of the correlators

In this work we use exclusively the local discretizations of the operators introduced in the previous subsection. Therefore, the expression of the bare operators in the lattice theory is the same as in Eq. (1). These bare operators are first O(a) improved and then renormalized. While the bare pseudoscalar density is by itself O(a) improved, the improvement of the vector and axial-vector currents takes the form

$$A_\mu^{\mathrm{imp},b}(x) = A_\mu^b(x) + ac_A(g_0^2)\widetilde{\partial}_\mu P^b(x), \qquad (21)$$

$$V_\mu^{\mathrm{imp},b}(x) = V_\mu^b(x) + ac_V(g_0^2)\widetilde{\partial}_\nu T_{\mu\nu}(x), \qquad (22)$$

where $T_{\mu\nu}^a(x) \equiv -\frac{1}{2}\bar{\psi}[\gamma_\mu,\gamma_\nu]\frac{\tau^a}{2}\psi$ is the tensor current. For the derivative $\widetilde{\partial}_\mu$, we use the symmetrized version of the lattice discretized derivative, namely

$$\widetilde{\partial}_\mu f(x) = \frac{1}{2a}(f(x + a\hat{\mu}) - f(x - a\hat{\mu})). \qquad (23)$$

The nonperturbatively calculated coefficient c_A was taken from Ref. [16], and the coefficient c_V from Ref. [17].

The finite renormalization of the vector and the axial-vector currents is performed with the nonperturbatively determined renormalization factors $Z_V(g_0^2)$ and $Z_A(g_0^2)$, supplemented by a quark-mass dependent factor in order to fully realize O(a) improvement; details are provided in Appendix A.

The pseudoscalar density $P^a(x)$ acquires a scale (and scheme) dependence via the process of renormalization. The renormalization factor is notated $Z_P(g_0^2, a\mu)$. Here, we renormalize $P^a(x)$ in the (nonperturbative) gradient-flow (GF) scheme at the renormalization scale μ where the corresponding coupling $\bar{g}_{\mathrm{GF}}^2 = 9.25$; this corresponds to a low scale of $\mu \approx 230$ MeV [18]. While none of our physics applications relies on the choice of a specific scheme, we note that in the latter publication, the scale dependence of the renormalization factor has been computed up to perturbative scales μ; thereby the connection to the renormalization-group invariant operator is known.

The renormalization of the PCAC mass is defined to preserve the axial Ward identity (2). Thus, all renormalization-scale dependent quantities in this paper are quoted in the aforementioned gradient-flow scheme. In particular the PCAC mass is renormalized by multiplying it with Z_A/Z_P, and the combination $m_\pi^2 f_\pi^2/m_{\mathrm{PCAC}}$ considered in Sec. V A via the factor $Z_A Z_P$. The numerical values of the renormalization factors are collected in Appendix A.

D. Numerical setup

Our calculations are performed on an $N_\mathrm{f} = 2 + 1$ ensemble with tree-level $\mathcal{O}(a^2)$-improved Lüscher-Weisz gauge action and nonperturbatively $\mathcal{O}(a)$-improved Wilson fermions [19]. The action corresponds to the choice of the Coordinated Lattice Simulations (CLS) initiative [20] and the bare parameters match those of the CLS zero-temperature ensemble E250 [21]. The latter are listed in Table I, together with the lattice spacing as determined in Ref. [22]. The time direction admits thermal boundary conditions with $N_\tau = 24$, which is the only difference relative to the zero-temperature ensemble, resulting in a temperature

TABLE I. Parameters and lattice spacing of the ensemble analyzed in this paper. The lattice spacing determination is from Ref. [22].

β/a	L/a	$6/g_0^2$	κ_l	κ_s	a [fm]
24	96	3.55	0.137232867	0.136536633	0.06426(76)

$$T = \frac{1}{\beta} = \frac{1}{24a} = 127.9(1.5) \text{ MeV.} \qquad (24)$$

Note that, assuming a pseudocritical temperature $T_{pc} = 156.5(1.5)$ MeV in $(2 + 1)$-flavor QCD [1], our temperature corresponds to $T/T_{pc} \approx 0.82$. For reference, we also quote the zero-temperature pseudoscalar masses and pion decay constant, determined in Ref. [23],

$$T = 0: \quad m_\pi^0 = 128.1(1.3)(1.5) \text{ MeV,}$$
$$m_K^0 = 488.98(0.3)(5.8) \text{ MeV,} \qquad (25)$$

$$f_\pi^0 = 87.4(0.4)(1.0) \text{ MeV,} \qquad (26)$$

where the first error is from the corresponding quantity in lattice units, and the second is from the lattice spacing determination of Ref. [22].

The ensemble has been generated using version 2.0 of the openQCD package [24], applying a small twisted mass to the light quark doublet for algorithmic stability. The correct QCD expectation values are obtained including the reweighting factors[1] for the twisted mass and for the Rational Hybrid Monte Carlo (RHMC) algorithm approximation used to simulate the strange quark. Measurements are performed on a single chain of 1200 configurations, each separated by four Molecular Dynamics Units (MDUs).

III. RESULTS ON THE PSEUDOSCALAR SECTOR

In this section, we present our lattice results on observables in the pseudoscalar sector, i.e. those related to pion properties. As an important reference quantity, we begin with the determination of the average (u, d) PCAC mass.

A. The PCAC mass

The extraction of the PCAC mass as defined in Eq. (4) is carried out by performing a fit to a constant in the range where a plateau is observed; see Fig. 1. Due to the longer plateau, the fit is performed along the x_3 direction. We obtain

$$\frac{m_{\mathrm{PCAC}}}{T} = 0.035(1). \qquad (27)$$

The PCAC mass obtained from the x_0 direction is compatible with the one obtained from the x_3 direction, pointing

---

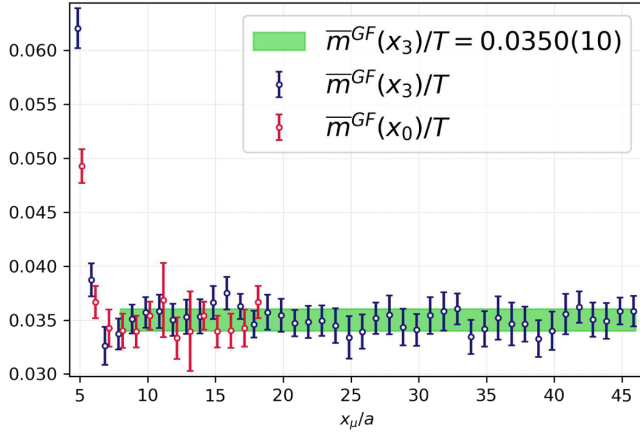[1]We have not found any negative reweighting factors.

FIG. 1. Renormalized PCAC mass in the E250 ensemble along the x_3 direction. The final result—obtained from a fit along the x_3 direction—is also shown with a 1-σ band. We have used the improved axial current together with the symmetrized derivative [see Eqs. (21)–(23)].

to cutoff effects at this value of the lattice spacing being small.

B. Static correlators: The pion screening mass and decay constant

In this subsection, we describe how the screening pion mass m_π and the screening decay constant f_π can be calculated. In order to accomplish this, we make use of the asymptotic behavior of the axial-current screening correlator, Eq. (5).

Making use of the PCAC-based relation (8) and of the symmetry of the correlators around $x_3 = L/2$, a one-state fit ansatz for the corresponding correlation functions can be formulated in the form

$$G_A^s(x_3, T) = \frac{A_1^2 m_1}{2} \cosh[m_1(x_3 - L/2)], \quad (28)$$

$$G_P^s(x_3, T) = -\frac{A_1^2 m_1^3}{8 m_{\mathrm{PCAC}}^2} \cosh[m_1(x_3 - L/2)], \quad (29)$$

$$G_{AP}^s(x_3, T) = -\frac{A_1^2 m_1^2}{4 m_{\mathrm{PCAC}}} \sinh[m_1(x_3 - L/2)]. \quad (30)$$

The pion screening mass m_π and f_π are obtained from the fit parameters m_1 and A_1 (derived in Appendix B) via

$$m_\pi = m_1, \qquad f_\pi = A_1 \sqrt{\sinh(m_1 L/2)}. \quad (31)$$

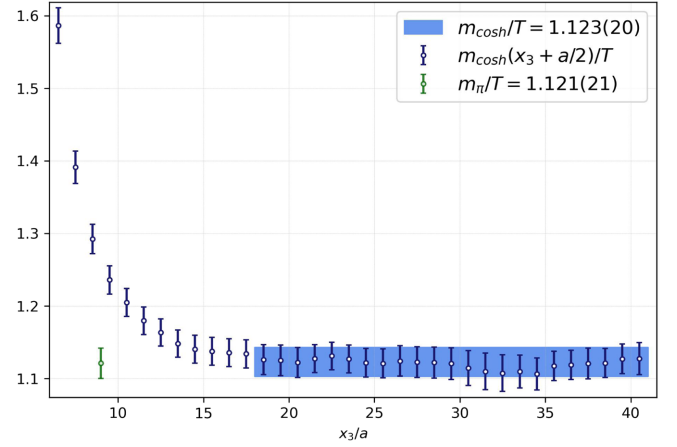The "cosh mass" with argument $(x_3 + a/2)$ is defined as the positive root of the following equation,

FIG. 2. Effective mass plot for the cosh mass $m_{\mathrm{cosh}}(x_3)$ as a function of the x_3 coordinate, obtained from the pseudoscalar screening correlation function at zero spatial momentum $G_P^s(x_3, T)$. It is assumed that the effective mass plateau starts at $x_3/a = 18$. The result of the fit to the effective mass values is represented by a 1-σ band. For comparison the value for the screening pion mass m_π, obtained from the fit of the pseudoscalar correlator is also included.

$$\frac{G_P^s(x_3, T)}{G_P^s(x_3 + a, T)} = \frac{\cosh[m_{\mathrm{cosh}}(x_3 + a/2) \cdot (x_3 - L/2)]}{\cosh[m_{\mathrm{cosh}}(x_3 + a/2) \cdot (x_3 + a - L/2)]}. \quad (32)$$

It is visualized in Fig. 2. Note that there is a different equation and a different solution for m_{cosh} for each value of x_3. The fits are performed using the Levenberg-Marquardt's method [25] and the results are shown in Fig. 3.

Due to its better signal-to-noise ratio, the screening pion mass m_π was first extracted using $G_P^s(x_3, T)$. Since neighboring correlator points are highly correlated, we have fitted only every second point (see also the procedure in Ref. [26]). Proceeding in this way, the dimension of the covariance matrix is reduced, enabling us to perform correlated fits over a longer physical range of distances. We have checked that fitting the complementary set of points in the interval gives a compatible result and averaging these two fit results does not lead to a smaller error (see Appendix E). In order to be sure that the ground state is isolated, we have repeated the fit to the correlation function for different fit windows, leaving out points that are furthest away from the correlator middle point $x_3 = L/2$. Our final result

$$m_\pi/T = 1.121(21), \quad (33)$$

corresponds to $m_\pi = 143(3)$ MeV. It is reported in Table II and is stable under small variations of the fit interval and corresponds to a correlated $\chi^2/\mathrm{d.o.f.} = 1.05$, where the degrees of freedom (d.o.f.) = 9. Furthermore, our final value for m_π is in very good agreement with the averaged
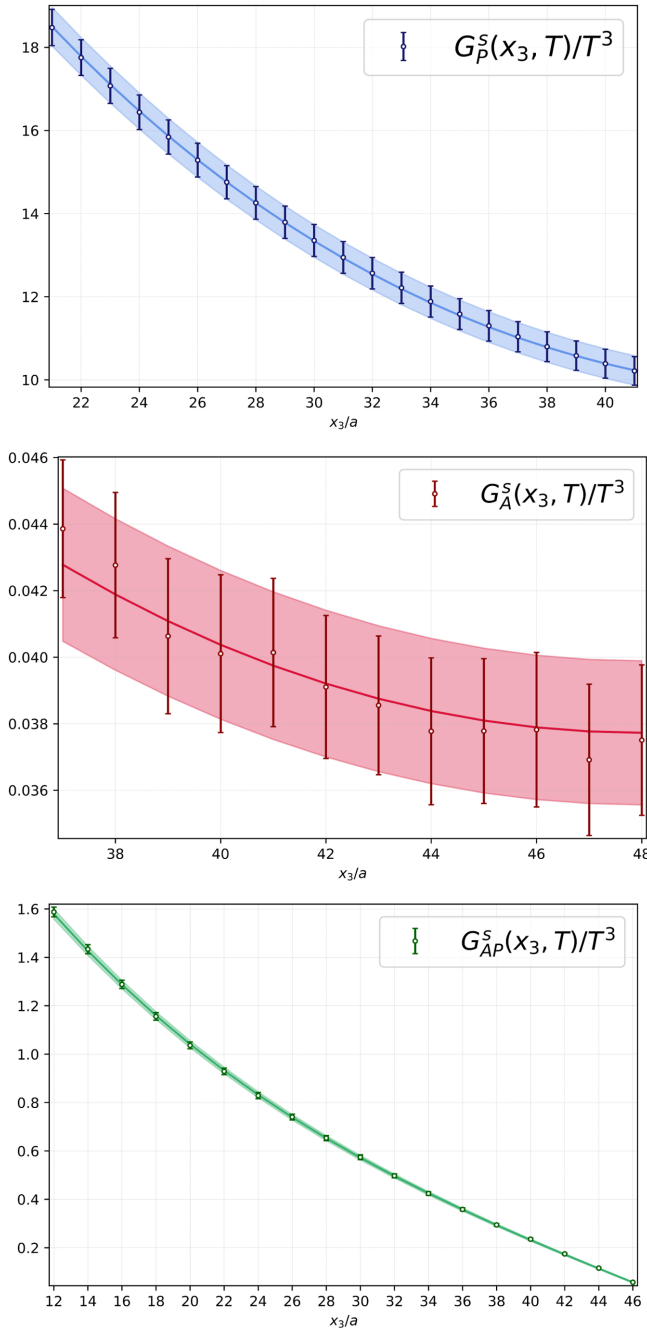
TABLE II. Summary of the results of the E250 thermal ensemble with $N_\tau = 24$. The pion quasiparticle mass ω_0 is calculated using $\omega_0 = u_m m_\pi$.

m_π/T	1.121(21)
f_π/T	0.559(11)
u_f	0.787(16)
u_m	0.786(18)
u_f/u_m	1.001(27)
ω_0/T	0.881(23)
f_π^t/T	0.710(16)
$\mathrm{Res}(\omega_0)/T^4$	0.392(21)

By repeating the procedure for different fit windows in an analogous manner, we note that the mean value is stable under small variations of the fit window and we select the final value for A_1 by choosing a fit which has a correlated $\chi^2/\text{d.o.f.} = 1.14\,(\text{d.o.f.} = 9)$ for $G_A^s(x_3, T)$ and $\chi^2/\text{d.o.f.} = 0.98\,(\text{d.o.f.} = 15)$ for $G_{AP}^s(x_3, T)$. Employing Eq. (B5) the value $f_\pi/T = 0.558(14)$, respectively, $f_\pi/T = 0.559(11)$ can be extracted for the screening pion decay constant. The latter value is selected as the final one and reported in Table II. The screening pion decay constant $f_\pi = 72(1)$ MeV is significantly lower than the pion decay constant $f_\pi^0 = 87.4(1.0)$ MeV [27] on the corresponding zero temperature ensemble.[2] The procedure for calculating the statistical error of the screening quantities m_π and f_π is described in Appendix D.

C. Properties of the pion quasiparticle

The results for the estimators u_m and u_f defined in Eqs. (17) and (18) together with the estimators for the screening quantities are presented in Table II. Good agreement is found for the two independent estimators u_f and u_m of the pion velocity. Both of them differ significantly from unity, which clearly represents a breaking of Lorentz invariance due to thermal effects. Additionally, we found that the zero-temperature pion mass given in Eq. (25) "splits" into a lower pion quasiparticle mass, $\omega_0 = 113(3)$ MeV, and a higher pion screening mass, $m_\pi = 143(3)$ MeV. The quasiparticle decay constant $f_\pi^t = f_\pi/u_m = 91(2)$ MeV is much closer to the vacuum decay constant f_π^0.

D. Dependence of the pion velocity u_f on a finite pion thermal width $\Gamma(T)$

The analysis of Son and Stephanov [10,11] concluded that at temperatures below the chiral phase transition, the imaginary part of the pion pole is parametrically small compared to its real part. In this subsection, we investigate

FIG. 3. Top panel: renormalized screening correlation function $G_P^s(x_3, T)/T^3$ and the result of the fit. The chosen fit interval is $x_3/a \in [21, 41]$. Middle panel: renormalized screening correlation function $G_A^s(x_3, T)/T^3$ and the result of the fit with a prior from $G_P^s(x_3, T)$. The chosen fit interval in this case is $x_3/a \in [37, 48]$. Bottom panel: renormalized screening correlation function $G_{AP}^s(x_3, T)/T^3$ and the result of the fit with a prior from $G_P^s(x_3, T)$. The chosen fit interval in this case is $x_3/a \in [12, 46]$.

value of the "cosh mass" $m_{\text{cosh}} = 1.123(20)$; see Fig. 2. The obtained fit parameters of $G_P^s(x_3, T)$ are then used as a prior to fit $G_A^s(x_3, T)$ and $G_{AP}^s(x_3, T)$.

---

[2]Note that in this work a different convention for the pion decay constant is followed resulting in an additional factor $\sqrt{2}$.

the sensitivity of our results for the pion quasiparticle mass and velocity parameter u to the assumption of a negligible thermal width of this quasiparticle. In order to examine the

$$\rho_{A_0}(\omega, T) = f_\pi^2 m_\pi^2 \frac{\Gamma(T)}{\pi} \frac{1}{2\omega_0} \left(\frac{1}{(\omega - \omega_0)^2 + \Gamma(T)^2} - \frac{1}{(\omega + \omega_0)^2 + \Gamma(T)^2} \right) + \dots, \tag{34}$$

where the second term is needed to ensure the antisymmetry of the spectral function in ω [15]. Expressing the correlator midpoint of the time-dependent Euclidean correlator $G_{A_0}(\beta/2, T)$ in terms of the spectral function ρ_{A_0} with the help of Eq. (14) and using $\omega_0 = u_f m_\pi$ one can extract the pion velocity u_f for different thermal pion widths $\Gamma(T) \in \{15, 30, 60\}$ MeV. The results are shown in Table III.

We find that the extracted estimator of the pion velocity $u_f = 0.787(16)$ (assuming the presence of a discrete delta term in the spectral function) is consistent with a Breit-Wigner approach up to pion thermal widths $\Gamma(T) \approx 30$ MeV.

E. Spectral function reconstruction with the Backus-Gilbert method

In order to extract the spectral function $\rho_{A_0}(\omega)$ at zero momentum from the corresponding temporal Euclidean correlator, $G_{A_0}(\tau_i, T), \tau \equiv x_0$, one has to invert the analog for G_{A_0} of Eq. (14) with a kernel $K(\tau_i, \omega) = \cosh(\omega(\beta/2 - \tau_i))/\sinh(\omega\beta/2)$, encountering a numerically ill-posed problem. A possible approach dealing with this task is the Backus-Gilbert method [28]. We adopt the notation of Ref. [13], where the method has first been applied to lattice QCD. It should be emphasized that, with this approach, no particular ansatz needs to be made for the spectral function. The Backus-Gilbert method provides an estimator for the smeared axial spectral function,

$$\hat{\rho}_{A_0}(\bar{\omega}) = \sum_{i=1}^{N_\tau} q_i(\bar{\omega}) G_{A_0}(\tau_i)$$
$$= \sum_{i=1}^{N_\tau} q_i(\bar{\omega}) \int_0^\infty d\omega \, K(\tau_i, \omega) \rho_{A_0}(\omega), \tag{35}$$

built from the lattice correlator data $G_{A_0}(\tau_i)$. Note that the coefficients q_i depend on some reference value $\bar{\omega}$ around which the so-called resolution function (or averaging kernel),

TABLE III. Dependence of the pion velocity u_f on a finite pion thermal width $\Gamma(T)$.

$\Gamma(T)$ [MeV]	u_f
15	0.783(19)
30	0.762(18)
60	0.671(21)

consequences of a finite thermal pion width on the pion velocity u we replace the δ distribution in Eq. (19) by a Breit-Wigner peak of width $\Gamma(T)$ resulting in

$$\hat{\delta}(\bar{\omega}, \omega) = \sum_{i=1}^{N_\tau} q_i(\bar{\omega}) K(\tau_i, \omega), \tag{36}$$

is concentrated. It is normalized according to

$$\int_0^\infty d\omega \, \hat{\delta}(\bar{\omega}, \omega) = 1. \tag{37}$$

Since the kernel $K(\tau_i, \omega)$ has a singularity in the limit $\omega \to 0$, it is advantageous to introduce a rescaling function

$$f(\omega) = \tanh(\omega\beta/2), \tag{38}$$

redefining the regularized kernel to be $K_f(\tau_i, \omega) = f(\omega) K(\tau_i, \omega)$. This allows us to rewrite Eq. (35) for the smeared and rescaled spectral function as

$$\frac{\hat{\rho}_{A_0}(\bar{\omega})}{f(\omega)} = \int_0^\infty d\omega \, \hat{\delta}(\bar{\omega}, \omega) \frac{\rho_{A_0}(\omega)}{f(\omega)}. \tag{39}$$

Inspecting Eq. (39), the desirable resolution function would be a Dirac delta distribution centered at $\bar{\omega}$. However, it has to satisfy Eq. (36) at the same time. In order to make the resolution function as sharply centered around $\bar{\omega}$ as possible, we minimize the second moment of its square subject to the constraint in Eq. (37). Therefore we minimize the following functional,

$$\mathcal{F}[q_i(\bar{\omega})]$$
$$= \int_0^\infty d\omega (\omega - \bar{\omega})^2 [\hat{\delta}(\bar{\omega}, \omega)]^2 - \alpha \left(\int_0^\infty d\omega \, \hat{\delta}(\bar{\omega}, \omega) - 1 \right),$$
$$= \sum_{i,j=1}^{N_\tau} q_i(\bar{\omega}) \left[\int_0^\infty d\omega K_i(\tau_i, \omega)(\omega - \bar{\omega})^2 K_j(\tau_j, \omega) \right] q_j(\omega)$$
$$- \sum_{i=1}^{N_\tau} \alpha \left(q_i(\bar{\omega}) \int_0^\infty d\omega K_i(\tau_i, \omega) - 1 \right),$$
$$\equiv \sum_{i,j=1}^{N_\tau} q_i(\bar{\omega}) W_{ij}(\bar{\omega}) q_j(\bar{\omega}) - \sum_{i=1}^{N_\tau} \alpha(q_i(\bar{\omega}) R_i(\bar{\omega}) - 1), \tag{40}$$

with α being a Lagrange multiplier. In practice the matrix $W_{ij}(\bar{\omega})$ is very close to being singular and needs a regularization procedure,
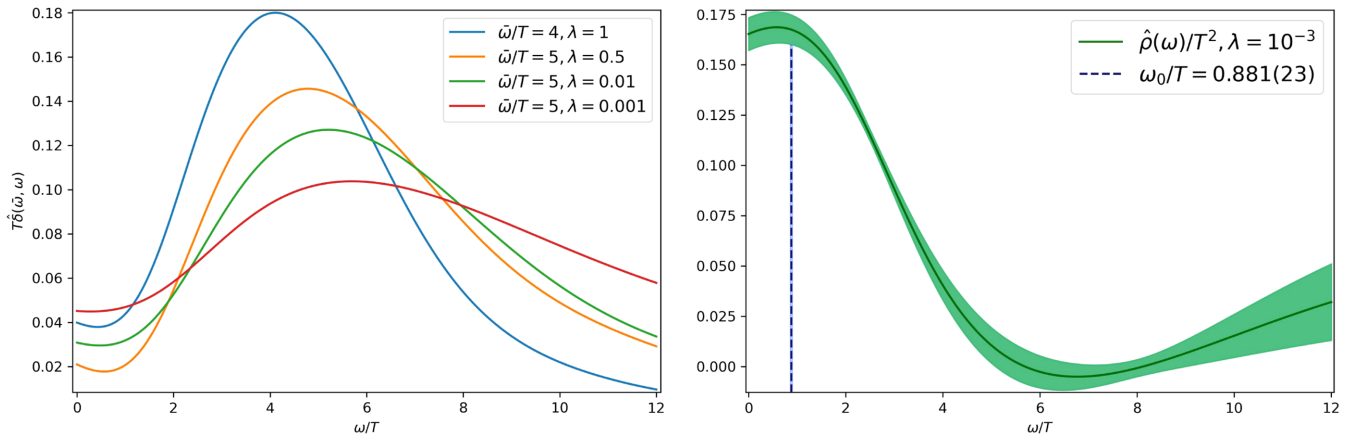
FIG. 4. Left panel: some examples of resolution functions for different values of λ, centered around $\bar{\omega}/T$. Right panel: estimator of the spectral function $\hat{\rho}_{A_0}(\omega, T)/T^2$. The blue dashed line corresponds to the location of the expected position of the pole ω_0 according to Eq. (15).

$$W_{ij}(\bar{\omega}) \rightarrow W_{ij}^{\mathrm{reg}}(\bar{\omega}) = \lambda W_{ij}(\bar{\omega}) + (1-\lambda)\mathrm{Cov}[G_{A_0}]_{ij},$$
$$0 < \lambda < 1. \tag{41}$$

The resulting coefficients that minimize Eq. (40) are then given by

$$q_j(\bar{\omega}) = \frac{\sum_{k=1}^{N_\tau} (W^{\mathrm{reg}}(\bar{\omega})^{-1})_{jk} R_k}{\sum_{i,l=1}^{N_\tau} R_i (W^{\mathrm{reg}}(\bar{\omega})^{-1})_{il} R_l}. \tag{42}$$

The values of λ quoted below refer to units in which all dimensionful quantities are turned into dimensionless ones by appropriate powers of temperature. Some examples for the resolution function $T\hat{\delta}(\bar{\omega}, \omega)$ for different values of λ are shown in the left panel of Fig. 4. The right panel of Fig. 4 shows the smeared and rescaled axial spectral function $\hat{\rho}_{A_0}(\bar{\omega}, T)/T^2$ with $\lambda = 10^{-3}$. It demonstrates model independently that the axial-charge correlator is dominated by low frequencies. Furthermore, the predicted position of the quasiparticle mass ω_0 is close to the peak of the smeared spectral function.

F. Comparison with results from the literature

Comparing our pion quasiparticle mass $\omega_0(T)$ and quasiparticle decay constant $f_\pi^t(T)$ at $T = 128$ MeV to the matching quantities at the corresponding zero temperature ensemble we get $\omega_0(T)/m_\pi^0 = 0.880(25)$ and $f_\pi^t(T)/f_\pi^0 = 1.039(26)$. Thus, the quasiparticle mass decreases at finite temperature while the quasiparticle decay constant increases. This behavior is similar to what is found in a ChPT calculation at two loops (see Ref. [8], Figs. 3 and 4). The reduction of the quasiparticle mass therein is ≈ 0.9. On the other hand the quasiparticle decay constant increases by a factor of approximately 1.06.

Regarding the screening pion mass m_π, we found that it increases with temperature compared to m_π^0. The ratio is $m_\pi/m_\pi^0 = 1.125(27)$. This statement is also supported by the study of Son and Stephanov near the chiral phase transition [10]. The screening mass that we obtained is larger than what one would expect based on a short linear extrapolation to $T = 128$ MeV using the continuum extrapolated data presented in a study with $N_f = 2 + 1$ highly improved staggered fermions in Ref. [26]. However, we note that their study does not have any lattice data for the temperature that we used.

In the recent publication [29], the authors work out the pion damping width and the pion spectral function in the framework of a $SU(2)$ Nambu-Jona-Lasinio (NJL) model for a few temperatures below the critical temperature $T_c^{\mathrm{NJL}} = 190$ MeV. They observe that the position of the peak of the pion spectral function at vanishing momentum $\mathbf{p}$ is moving to the right for increasing temperatures $T/T_c^{\mathrm{NJL}} \in \{0, 0.79, 0.89, 0.97\}$ [see Fig. 3 in [29]]. This contradicts our observation of the pion pole mass being reduced at finite temperature.

IV. QUARK NUMBER SUSCEPTIBILITY

With $\mathcal{N}_q = \int \mathrm{d}^3 x V_0(0, \mathbf{x})$, V_0 being the time component of the local vector current,[3] the usual definition of the quark number susceptibility (QNS) for a given flavor is given by

$$\chi_q(T) = \left.\frac{\partial \rho_q}{\partial \mu_q}\right|_{\mu_q=0}. \tag{43}$$

It measures the response of the quark number density,

---

[3]Note the additional normalization factor $1/2$ resulting in an overall factor of $1/2$ for the correlator and therefore also for the QNS.
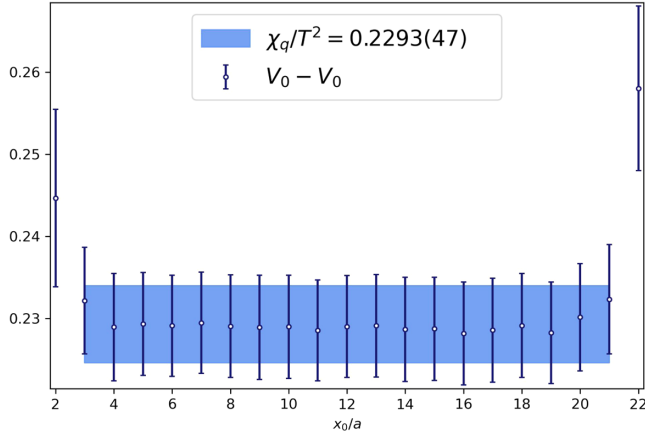
FIG. 5. Quark number susceptibility extracted from the local vector current correlator, Eq. (45). The mean and error have been obtained from a correlated fit in the range [3,21].

$$\rho_q = \frac{1}{V}\frac{\mathrm{Tr}[\mathcal{N}_q e^{-\beta(\mathcal{H}-\mu_q\mathcal{N}_q)}]}{\mathrm{Tr}[e^{-\beta(\mathcal{H}-\mu_q\mathcal{N}_q)}]} = \frac{\langle\mathcal{N}_q\rangle}{V}, \qquad (44)$$

to an infinitesimal change in the quark chemical potential $\mu_q \to \mu_q + \delta\mu_q$.

On the lattice, we define the quark number susceptibility as

$$\chi_q(x_0, T) = Z_V^2(g_0^2)\beta \int \mathrm{d}^3x \langle V_0^a(x_0,\mathbf{x})V_0^a(0,\mathbf{0})\rangle, \qquad x_0 \neq 0. \tag{45}$$

Note, that for the QNS no improvement of the vector current is needed.

The result is shown in Fig. 5 in temperature units. Please note that we are not including any contributions from disconnected diagrams in our result for the QNS and in this approximation it is proportional to the isospin susceptibility. In Ref. [30] (see Table I) the quark number susceptibility was determined as a function of the temperature using $2 + 1$ dynamical staggered quark flavors and, additionally, a continuum extrapolation was done. Taking into account the different normalization factor, their results are $\chi_q(T)/T^2 = 0.216(46)$ and $\chi_q(T)/T^2 = 0.241(44)$ for the temperatures $T = 125$ MeV and $T = 130$ MeV, respectively (see Table I of Ref. [30]). Our result, $\chi_q(T)/T^2 = 0.2293(47)$ is compatible with both of these results. Although we did not perform a continuum extrapolation, our lattice spacing is around $2/3$ of the finest lattice spacing employed in Ref. [30], so beside the larger errors of the results from Ref. [30], the presence of only small cutoff effects may also explain the good agreement. Next, we are going to compare our lattice estimate for the QNS with the HRG model and also test an alternative HRG employing our modified dispersion relation for the pion quasiparticle.

A. Comparison with the hadron resonance gas model

The HRG model [31,32] describes the thermodynamic properties and the quark number susceptibilities of the low-temperature phase rather well. It assumes that the thermodynamic properties of the system are given by the sum of the partial contributions of noninteracting hadron species, i.e.

$$\ln[Z(T, V)] = -\frac{V}{2\pi^2}\sum_i \int_0^\infty \mathrm{d}p\, p^2 \ln\left[1 - \eta_i e^{-\sqrt{m_i^2+\mathbf{p}^2}/T}\right], \tag{46}$$

where $\eta_i = \pm 1$ takes into account bosons and baryons, respectively. The sum extends over all resonances up to a mass of 2.0 GeV, since for most of them the width is not large compared to the temperature.

The quark number susceptibility can be obtained as the sum [33]

$$\chi_q(T) = (\chi_q)_{\mathrm{mesons}} + (\chi_q)_{\mathrm{baryons}}, \tag{47}$$

where

$$\frac{(\chi_q)_{\mathrm{mesons}}}{T^2} = \frac{2\beta^3}{3}\sum_{\mathrm{multiplets}}(2J+1)I(I+1)(2I+1)$$
$$\times \int \frac{\mathrm{d}^3\mathbf{p}}{(2\pi)^3}f_\mathbf{p}^B(1+f_\mathbf{p}^B), \tag{48}$$

$$\frac{(\chi_q)_{\mathrm{baryons}}}{T^2} = \frac{2\beta^3}{3}\sum_{\mathrm{multiplets}}(2J+1)I(I+1)(2I+1)$$
$$\times \int \frac{\mathrm{d}^3\mathbf{p}}{(2\pi)^3}f_\mathbf{p}^F(1-f_\mathbf{p}^F), \tag{49}$$

and $f_\mathbf{p}^{B/F} = 1/[e^{\beta\omega_\mathbf{p}} \mp 1]$ are the Bose-Einstein and Fermi-Dirac distributions. The sums are carried out over all multiplets of spin J and isospin I that are not identical. Especially particles and antiparticles have to be considered separately. This results in an additional factor of two in the baryon case and for mesons with strange quark constituents. An alternative to the HRG model is to only include the pion contribution, however taking into account the modified dispersion relation (15) at low momenta,

$$\frac{\chi_q}{T^2} = 4\beta^3 \int_{|\mathbf{p}|<\Lambda_p} \frac{\mathrm{d}^3\mathbf{p}}{(2\pi)^3}f_\mathbf{p}^B(\omega_\mathbf{p})(1+f_\mathbf{p}^B(\omega_\mathbf{p})), \tag{50}$$

where $\Lambda_p = 400$ MeV is about the momentum scale at which the predictions of the thermal chiral effective theory were seen to break down in Ref. [13]. Note that in this model the sum over the resonances is absent. The contributions of the other hadrons are taken into account indirectly via the modified dispersion relation, since the collisions of the pions among themselves and with other
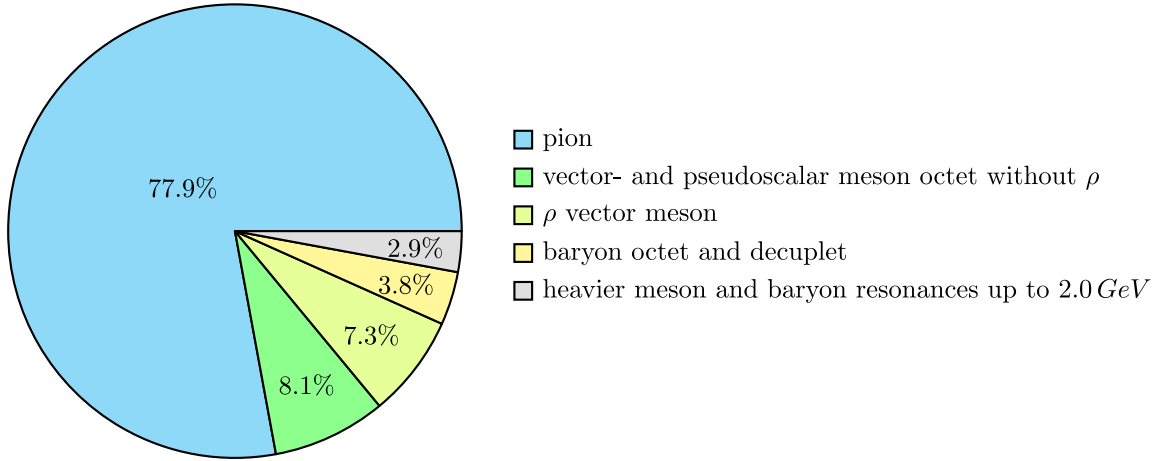
FIG. 6. Relative composition of the total quark number susceptibility predicted by the hadron resonance gas model.

hadrons give rise to the modified pion dispersion relation. Employing Eqs. (48) and (49) within the HRG model, summing all resonances up to a mass of 2 GeV, one obtains $\chi_q(T)/T^2 = 0.2428$, which is 5.8% above our lattice estimate $\chi_q(T)/T^2 = 0.2293(47)$.

In the HRG model the pion contributes $\chi_q/T^2\big|_{\text{pion}} = 0.1890$ corresponding to 77.9% of the total QNS followed by a contribution of 15.4% of the vector and pseudoscalar meson octets (7.3% of this is attributable to the ρ vector meson). The baryon octet and decuplet contributes 3.8%, the largest portion (2.5%) stemming from the Δ resonance due to the large spin degeneracy factor. Heavier meson and baryon resonances up to a mass of 2 GeV contribute the remaining 2.9% to the final result (Fig. 6). It is questionable whether resonances whose full width is higher than the temperature should be taken into account. For instance the $K_0^*(700)$ resonance has a full Breit-Wigner width (478 ± 50 MeV) of nearly four times the temperature and has therefore been neglected.

Making use of Eq. (50) with $u_m = 0.786$ and a screening pion mass $m_\pi = 143$ MeV one obtains $\chi_q(T)/T^2 = 0.2163$ which is 5.3% below the lattice estimate. At this point we have only integrated up to the momentum cutoff $\Lambda_p = 400$ MeV since it is not clear if the thermal width of the pion is still negligible for $|\mathbf{p}| > \Lambda_p$ and, as a consequence, including contributions from higher momenta may not be justified. However, this model is not very predictive as it depends very strongly on the choice of the momentum cutoff.

V. ORDER PARAMETERS FOR CHIRAL SYMMETRY RESTORATION

In this section, several order parameters for chiral symmetry restoration are investigated. Based on the screening pion quantities m_π^2 and f_π^2 presented in Sec. III, we first evaluate an "effective chiral condensate" based on the

Gell-Mann-Oakes-Renner relation. Additionally, we explore two Euclidean-time dependent thermal correlation functions that are order parameters for chiral symmetry and compare them to their zero-temperature counterparts. We begin with the (PA_0) correlator, which contains the pion pole that we have studied in Sec. III. We then consider the difference of the (isovector) vector and axial-vector correlators. In the QCD vacuum, the corresponding spectral functions are measured experimentally in τ decays [34]. They become degenerate in the chirally restored phase of QCD. Their temperature dependence in the chirally broken phase has been studied extensively in the framework of hadronic models supplemented by sum rules [35–37].

A. The GOR relation

Following Ref. [12], we introduce a "effective chiral condensate" based on the GOR relation,

$$\langle\bar\psi\psi\rangle_{\text{GOR}}^{\text{GF}} \equiv -\frac{f_\pi^2 m_\pi^2}{m_q}. \tag{51}$$

For $m_q \to 0$ it matches the actual chiral condensate. Additionally, since above T_c, $m_\pi \sim T$ and $f_\pi \sim m_q$, $\langle\bar\psi\psi\rangle_{\text{GOR}}^{\text{GF}}$ is of $\mathcal{O}(m_q T^2)$. Thus, it serves as an order parameter for chiral symmetry. Using $m_q = m_{\text{PCAC}}$ and the screening quantities of Table II we obtain

$$|\langle\bar\psi\psi\rangle_{\text{GOR}}^{\text{GF}}|^{1/3} = 286(5) \text{ MeV}. \tag{52}$$

The value of the chiral condensate has been extracted in the gradient flow scheme just like the PCAC mass (see Sec. II C). Comparing with the chiral condensate on the corresponding zero-temperature ensemble [23], we get

$$\left[\frac{\langle\bar\psi\psi\rangle_{T\approx128\text{ MeV}}}{\langle\bar\psi\psi\rangle_{T\approx0\text{ MeV}}}\right]_{\text{GOR}} \equiv \frac{(f_\pi^2 m_\pi^2)_{T\approx128\text{ MeV}}}{(f_\pi^2 m_\pi^2)_{T\approx0\text{ MeV}}} = 0.84(5), \tag{53}$$

which corresponds to a reduction by 16%. This reduction is compatible within the scope of the error with a three-loop result of Gerber and Leutwyler (see Ref. [6], Fig. 5).

B. The (PA_0) correlator

In Ref. [12] it was shown that the temporal (PA_0) correlator can be predicted exactly in the chiral limit,

$$G_{PA_0}(x_0, T) = \frac{\langle \bar{\psi}\psi \rangle}{2\beta}\left(x_0 - \frac{\beta}{2}\right). \quad (54)$$

As can be seen from Eq. (54) the (PA_0) correlator is antisymmetric around $\beta/2$. Consequently, we set the point $x_0 = 12a$ to zero. In our analysis we have averaged over the (PA_0) and (A_0P) correlator. The latter can be obtained interchanging source and sink. The estimator based on the last expression of Eq. (11) has the better signal-to-noise ratio. Since this correlator is proportional to the chiral condensate $\langle \bar{\psi}\psi \rangle$, it can serve as an order parameter for chiral symmetry restoration as well. Looking at the ratio of the thermal over reconstructed correlator [see Eq. (60)], we observe a slightly more pronounced reduction (Fig. 7) by a factor of $\approx 0.80(2)$ compared to the reduction by a factor of 0.84(5) that we had estimated using the Gell-Mann-Oakes-Renner reaction [see Eq. (53)].

C. Dey-Eletsky-Ioffe mixing theorem at finite quark mass

Let us consider the following real-time correlators at finite temperature T:

$$C_{\mu\nu}^{J,a,b}(q,T) = \frac{i\delta^{ab}\int \mathrm{d}^4 x\, e^{iqx}\sum_n \langle n|\mathbb{T}\{J_\mu^a(x)J_\nu^b(0)\}e^{-H/T}|n\rangle}{\sum_n \langle n|e^{-H/T}|n\rangle}$$

$$(J \in \{V, A\}), \quad (55)$$

where the sum is over the full set of the eigenstates of the Hamiltonian H and $\{a, b\}$ are isospin indices. To order T^2 it is sufficient to account only for the contributions of the two lowest states in Eq. (55)—vacuum and one pion state. In Refs. [38–40] it was demonstrated, using PCAC current algebra, that the finite-temperature vector and axial-vector correlators can be described with the help of their vacuum counterparts. In terms of the corresponding spectral functions this statement reads

$$\rho_V(\omega, \mathbf{p}, T) = (1-\epsilon)\rho_V(\omega, \mathbf{p}, T=0) + \epsilon\rho_A(\omega, \mathbf{p}, T=0), \quad (56)$$

$$\rho_A(\omega, \mathbf{p}, T) = (1-\epsilon)\rho_A(\omega, \mathbf{p}, T=0) + \epsilon\rho_V(\omega, \mathbf{p}, T=0), \quad (57)$$

where $\epsilon \equiv T^2/(6(f_\pi^0)^2)$ is a temperature dependent expansion parameter in powers of the pion density. Notice that as
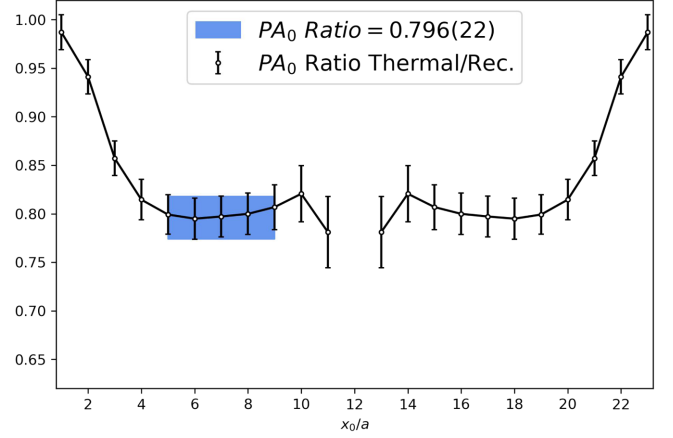

FIG. 7. Ratio of the temporal thermal (PA_0) correlator and the reconstructed correlator (PA_0) correlator. The errors on the ratio have been estimated using the jackknife method. The blue band shows the result from a correlated fit to the plateau.

a consequence of Eqs. (56) and (57) the sum of the vector and axial-vector spectral function does not change when the temperature is switched on. Furthermore, the difference is proportional to its zero-temperature equivalent:

$$\rho_V(\omega, \mathbf{p}, T) - \rho_A(\omega, \mathbf{p}, T)$$
$$= (1 - 2\epsilon)[\rho_V(\omega, \mathbf{p}, T=0) - \rho_A(\omega, \mathbf{p}, T=0)]. \quad (58)$$

As a consequence the above quantity serves as an order parameter for chiral symmetry restoration. Thus, in the following we will investigate its behavior even for nonzero quark mass. To do so, we consider the difference "$V - A$" of the corresponding $\mathcal{O}(a)$-improved temporal correlators projected to zero momentum

$$\delta^{ab}[G_V(x_0, T, \mathbf{p}=0) - G_A(x_0, T, \mathbf{p}=0)]$$
$$\equiv -\frac{1}{3}\int \mathrm{d}^3 x \sum_{i=1}^{3}[\langle V_i^a(x)V_i^b(0)\rangle - \langle A_i^a(x)A_i^b(0)\rangle]. \quad (59)$$

In order to obtain a comparable effectively zero-temperature quantity, we use the corresponding quasi zero-temperature E250 ensemble of size 192×96^3. This is achieved by calculating the "reconstructed" correlator $G_V^{\mathrm{rec}} - G_A^{\mathrm{rec}}$ for the difference, i.e. the thermal Euclidean correlator that would be realized if the spectral function was unaffected by thermal effects. Following a method first proposed in Ref. [41], we define our reconstructed correlators as

$$G_J^{\mathrm{rec}}(x_0, T, \mathbf{p}) = \sum_{m\in\mathbb{Z}} G_J(|x_0 + m\beta|, 0, \mathbf{p}) \quad (J \in \{V, A\}). \quad (60)$$
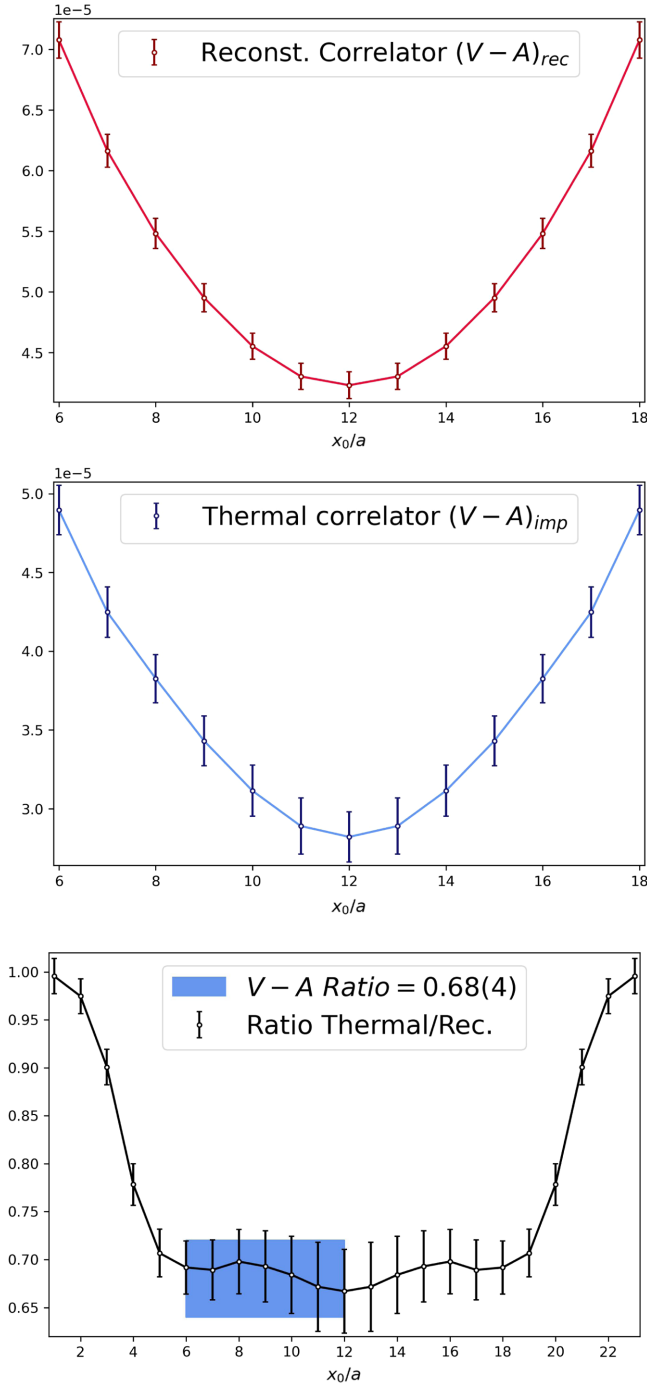
It is based on the identity of the kernel function

FIG. 8. Top panel: the reconstructed correlator for the difference "$V - A$." Middle panel: the difference of "$V - A$" at $T \approx 128$ MeV. Bottom panel: ratio of the difference "$V - A$" and the difference of the reconstructed correlator "$(V - A)_{\text{rec}}$." The errors on the ratio have been estimated using the jackknife method. The blue band shows the result from a correlated fit to the plateau.

$$\frac{\cosh(\omega(\beta/2 - x_0))}{\sinh(\omega\beta/2)} = \sum_{m \in \mathbb{Z}} e^{-\omega|x_0 + m\beta|}. \qquad (61)$$

The top and middle panel of Fig. 8 shows the difference "$V - A$" for the thermal ensemble and the same quantity for

the reconstructed correlator. Their ratio is shown in the bottom panel of Fig. 8. For vanishing quark masses one would expect it to be flat consistent with Eq. (58) obtained in the chiral limit. However, since chiral symmetry restoration is a long-distance effect, one expects that for physical quark masses the suppression of the ($V - A$) spectral function happens mostly at low energies which translates to the longest (Euclidean) time accessible. This is consistent with the dip that we observe around the midpoint ($x_0 = 12$) in Fig. 8. Furthermore, the difference "$V - A$" shows a significant reduction by a factor of approximately 0.68 at $T \approx 128$ MeV. Therefore, chiral symmetry restoration is already at an advanced stage in the spectral function.

Summarizing our results, we find that the "effective chiral condensate," which is extracted from static screening quantities, is reduced by a factor of 0.84(5). This value is compatible within errors with the reduction of 0.80(2) seen in the temporal (PA_0) correlator, which, in the chiral limit, is proportional to the chiral condensate. On the other hand, the reduction of the temporal ($V - A$) correlator, 0.68(4), is more pronounced. The different rate at which different order parameters of chiral symmetry breaking approach zero already shows up in predictions from chiral perturbation theory at vanishing quark masses. Specifically the suppression of the chiral condensate to leading order in T^2 goes like $1 - \frac{T^2}{8(f_\pi^0)^2}$ (see Refs. [6,42]) and is therefore less pronounced relative to Eq. (58) with $1 - 2\epsilon = 1 - \frac{T^2}{3(f_\pi^0)^2}$ [38].

VI. CONCLUSION

In this work we have found that the zero-temperature pion mass "splits" into a lower pion quasiparticle mass ω_0 and a higher pion screening mass m_π at finite temperature, confirming the findings of Ref. [13] in QCD with two quark flavors (u, d). Our results are also in good quantitative agreement with existing predictions of chiral perturbation theory: see Secs. III F and V A. Additionally, we have computed the two temperature-dependent parameters which determine the modified dispersion relation of the pion quasiparticle in the low-temperature phase of QCD [see Eq. (15)]. An assumption in determining the pion-velocity parameter u was a discrete peak structure in the axial spectral function. Using instead a Breit-Wigner ansatz with a finite thermal width, we could confirm that—within the statistical error—our estimator of the pion velocity u_f is stable within about three percent up to a finite pion width $\Gamma(T) \approx 30$ MeV. We have further employed the Backus-Gilbert method to show, independently of any model, that the axial correlator is indeed dominated by low frequencies.

The quark number susceptibility computed on the lattice has been compared to the predictions of the hadron resonance gas model as well as to the estimate where only pions are taken into account, however using their modified dispersion relation. The lattice estimate is found to lie approximately in the middle between these two predictions.

Nonetheless, one should keep in mind the strong dependence on the momentum cutoff of the last approach. Hence, an analysis at nonvanishing momentum with a high resolution would be desirable in order to narrow down the validity of the chiral effective theory and, as a consequence, determine an appropriate value of the momentum cutoff Λ_p more precisely.

Finally, we have investigated the degree of restoration of chiral symmetry in two different channels, namely the pseudoscalar one and in the difference of the (isovector) vector and axial-vector correlators $V - A$. We have done this by forming the ratio of the thermal correlator to the one reconstructed from the zero-temperature simulation. Quantitatively, we found the $V - A$ channel to exhibit a higher degree of chiral symmetry restoration.

Looking ahead, one might further ask if the relatively strong change in the pion screening quantities is due to its Goldstone-boson nature or if non-Goldstone hadrons are similarly modified by thermal effects [43]. We are generating a thermal ensemble with $N_\tau = 20$ and otherwise identical parameters. This choice corresponds to a temperature $T = 154$ MeV, just below the crossover regime.

APPENDIX A: RENORMALIZATION PROCESS

Following [47], we renormalize the correlators in the following way:

$$G_V^{\text{ren}} = Z_V^2(g_0^2)(1 + 2am_q b_V(g_0^2))G_V, \qquad (A1)$$

$$G_A^{\text{ren}} = Z_A^2(g_0^2)(1 + 2am_q b_A(g_0^2))G_A, \qquad (A2)$$

$$G_{A_0}^{\text{ren}} = Z_A^2(g_0^2)(1 + 2am_q b_A(g_0^2))G_{A_0}, \qquad (A3)$$

TABLE IV.   Summary of the renormalization parameters.

$Z_V(g_0^2)$	[17]	0.73453(6)
$Z_A(g_0^2)$	[48]	0.76900(42)
$Z_P(g_0^2)$	[18]	0.34768
$b_V(g_0^2)$	[17]	1.551(10)
$b_A(g_0^2)$	[47]	1.38(6)
$\kappa_{\text{cr.}}$	[17]	0.1371726(13)
κ_1	[27]	0.137232867

$$G_{PA_0}^{\text{ren}} = Z_P(g_0^2)Z_A(g_0^2)(1 + am_q b_A(g_0^2))G_{PA_0}, \qquad (A4)$$

$$G_P^{\text{ren}} = Z_P^2(g_0^2)G_P, \qquad (A5)$$

with $g_0^2 = 6/\beta$ being the bare gauge coupling and

$$am_q = \frac{1}{2}\left(\frac{1}{\kappa_1} - \frac{1}{\kappa_{\text{cr}}}\right) \qquad (A6)$$

being the bare subtracted quark mass. The values for the renormalization constants Z_J and the finite quark mass parameters b_J are given in Table IV.

APPENDIX B: EXTRACTING f_π OUT OF A_1

Let us denote the correlation function of a single state propagating forward as

$$c_f(x_3) = c_f^0 e^{-m_1 x_3}, \qquad (B1)$$

and analogously we denote the backward contribution as

$$c_b(x_3) = c_b^0 e^{-m_1(L-x_3)}. \qquad (B2)$$

Including the (tiny) contributions warping around the lattice the forward contribution becomes

$$\begin{aligned} c_f(x_3) &= c_f^0(e^{-m_1 x_3} + e^{-m_1(L+x_3)} + \ldots), \\ &= c_f^0 e^{-m_1 x_3} \sum_{n=0}^{\infty} e^{-nm_1 L}, \\ &= c_f^0 e^{-m_1 x_3} \frac{1}{1 - e^{-m_1 L}}. \end{aligned} \qquad (B3)$$

Combining forward and backward contributions and comparing with Eq. (28) we obtain

$$G_A^s(x_3, T) = \frac{A_1^2 m_1}{2} \cosh[(m_1(x_3 - L/2)]$$
$$= \frac{c_0}{1 - e^{-m_1 L}} \left(e^{-m_1 x_3} + e^{-m_1(L-x_3)} \right). \quad \text{(B4)}$$

Pulling out a factor of $e^{-m_1 L/2}$ and reading off $c_0 = \frac{1}{2} f_\pi^2 m_1$ from Eq. (5) we can finally link the screening pion decay constant f_π with the fit parameter A_1 as follows:

$$f_\pi = A_1 \sqrt{\sinh{(m_1 L/2)}}. \quad \text{(B5)}$$

APPENDIX C: CHIRAL EFFECTIVE THEORY LAGRANGIAN OF SON AND STEPHANOV

In the chiral effective theory approach of Son and Stephanov [10,11] the dynamics of the pions at finite temerpature is described by the Lagrangian,

$$\mathcal{L}_{\text{eff}} = \frac{f_t^2}{4} \langle \nabla_0 \Sigma \nabla_0 \Sigma^\dagger \rangle - \frac{f_\pi^2}{4} \langle \partial_i \Sigma \partial_i \Sigma^\dagger \rangle + \frac{m_\pi^2 f_\pi^2}{2} \text{Re} \langle \Sigma \rangle, \quad \text{(C1)}$$

where Σ denotes an $SU(2)$ matrix whose phase describes the pions, $\nabla_0 \Sigma = \partial_0 \Sigma - \frac{i}{2} \mu_{I5} (\tau_3 \Sigma + \Sigma \tau_3)$ is the covariant derivative, μ_{I5} denotes the axial isospin chemical potential and the trace is taken in flavor space. Note that in the presence of a thermal medium Lorentz invariance is broken resulting in two independent decay constants which are related through the pion velocity [10],
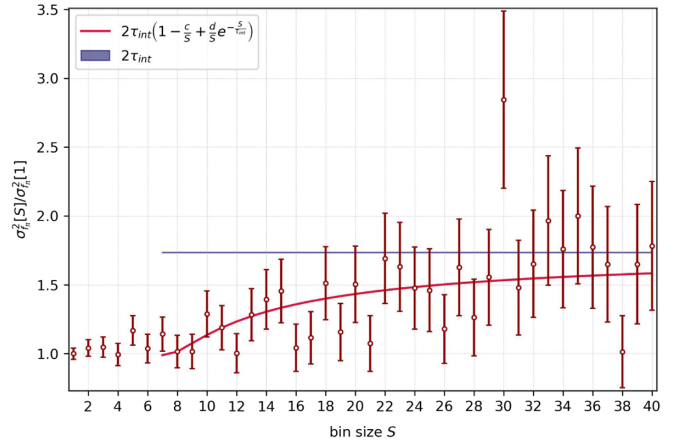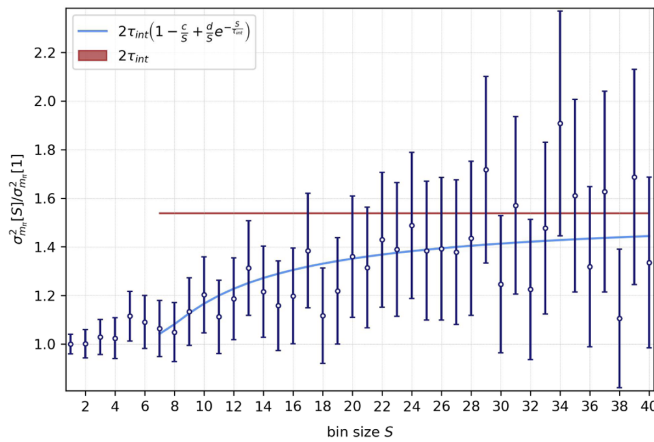
$$u = \frac{f_\pi}{f_t}. \quad \text{(C2)}$$

APPENDIX D: ERROR ANALYSIS

If $N_{\text{con}} = 1200$ denotes the number of configurations, then the mean value $\bar{O}$ of any lattice observable O can be obtained via

$$\bar{O} = \frac{1}{N_{\text{con}}} \sum_{i=1}^{N_{\text{con}}} O_i. \quad \text{(D1)}$$

All errors quoted in this work are purely statistical and estimated using *jackknife* resampling [49], where one first generates N_{con} jackknife replica

$$O_i^J = \frac{1}{N_{\text{con}} - 1} \sum_{j \neq i}^{N_{\text{con}}} O_j. \quad \text{(D2)}$$

Employing this procedure the error on the mean of any lattice observable can be calculated as

$$\sigma_{\bar{O}} = \sqrt{\frac{N_{\text{con}} - 1}{N_{\text{con}}} \sum_i (O_i^J - \bar{O})^2}, \quad \text{(D3)}$$

where the additional factor $(N_{\text{con}} - 1)$ arises due to the fact that the jackknife replicas are not statistically independent. Furthermore Eq. (D3) assumes uncorrelated jackknife replicas. However, since the configurations are obtained from Monte Carlo simulations the number of effectively independent jackknife replicas is [50]

$$N_{\text{ind}} = \frac{N_{\text{con}}}{2\tau_{O,\text{int}}}. \quad \text{(D4)}$$

FIG. 9. Left panel: normalized variance $\sigma_{m_\pi}^2[S]/\sigma_{m_\pi}^2[1]$ of the screening pion mass m_π in dependence of the bin size S. Right panel: normalized variance $\sigma_{f_\pi}^2[S]/\sigma_{f_\pi}^2[1]$ of the screening decay constant f_π in dependence of the bin size S. In both cases the fit function as well as its "infinite bin size extrapolation" for the integrated autocorrelation time $2\tau_{\text{int}}$ is shown.

Following Ref. [51], we estimate the integrated autocorrelation time $2\tau_{O,\mathrm{int}}$ as a fit parameter for the normalized variance using the fit ansatz

$$\frac{\sigma_O^2[S]}{\sigma_O^2[1]} = 2\tau_{O,\mathrm{int}}\left(1 - \frac{c}{S} + \frac{d}{S}e^{-\frac{S}{\tau_{O,\mathrm{int}}}}\right), \qquad O \in \{m_\pi, f_\pi\}. \tag{D5}$$

It corresponds to an asymptote for infinite bin size S (see Fig. 9). Therefore—to avoid an underestimation of the error—we quote

$$\hat{\sigma}_{\bar{O}} = \sqrt{2\tau_{O,\mathrm{int}}}\,\sigma_{\bar{O}}, \qquad O \in \{m_\pi, f_\pi\} \tag{D6}$$

as our final result. For the remaining observables discussed in this work, autocorrelation effects were taken into account using binning, i.e. averaging the data samples over a bin size $N_{\mathrm{bin}} = 20$,

$$O_i^B = \frac{1}{N_{\mathrm{bin}}} \sum_{j=N_{\mathrm{bin}}(i-1)+1}^{iN_{\mathrm{bin}}} O_j, \qquad i \in \left\{1, ..., \frac{N_{\mathrm{con}}}{N_{\mathrm{bin}}} = 60\right\}, \tag{D7}$$

before building the jackknife replicas O_i^J. Therefore, in this case, one has to replace $O_j \to O_j^B$ and $N_{\mathrm{con}} \to N_{\mathrm{con}}/N_{\mathrm{bin}}$ in Eq. (D2).

APPENDIX E: SYSTEMATICS FOR THE EXTRACTION OF THE SCREENING PION MASS m_π

In this appendix we examine the systematics of choosing the fit range for the extraction of the screening pion mass m_π. Figure 10 shows the extracted screening masses for different starting points of the fit interval. Our quoted value $m_\pi/T = 1.121(21)$ (see blue band in Fig. 10) obtained from the fit range [21,41] is compatible with all the results obtained using different fit ranges.
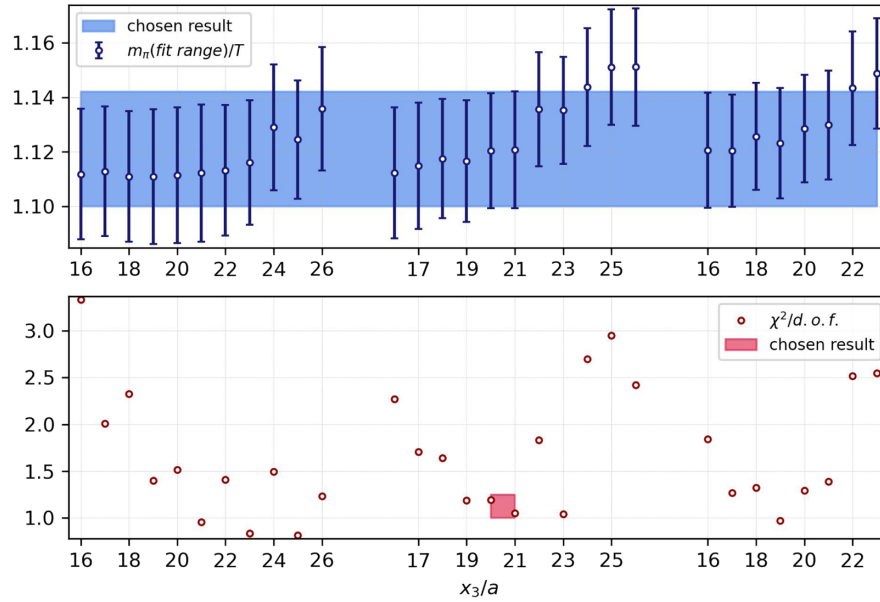

FIG. 10. Extracted screening masses m_π (top) and the corresponding correlated $\chi^2/\mathrm{d.o.f.}$ (bottom) for different fit ranges. The three blocks show the results of the fits with fit range lengths of 15, 21, and 25, respectively. In all cases only every second point is fitted as explained in Sec. III B.

APPENDIX F: NUMERICAL VALUES FOR TEMPORAL CORRELATORS

In this appendix we list the means and errors of the (anti)symmetrized temporal correlators used in this work (see Table V).

TABLE V. Temporal (anti)symmetrized correlators projected to zero momentum. All errors quoted are purely statistical. Since only the ratios are needed the correlators are not renormalized.

x_0/a	$G_{(V-A)_{\mathrm{imp}}}(x_0, T)$	$G_{(V-A)_{\mathrm{rec}}}(x_0, T)$	$G_{(PA_0)_{\mathrm{imp}}}(x_0, T)$	$G_{(PA_0)_{\mathrm{rec}}}(x_0, T)$
1	$1.754(1) \times 10^{-2}$	$1.76(3) \times 10^{-2}$	$2.323(5) \times 10^{-2}$	$2.35(2) \times 10^{-2}$
2	$1.392(3) \times 10^{-3}$	$1.43(3) \times 10^{-3}$	$4.63(2) \times 10^{-3}$	$4.92(5) \times 10^{-3}$
3	$2.78(2) \times 10^{-4}$	$3.09(6) \times 10^{-4}$	$1.58(2) \times 10^{-3}$	$1.85(2) \times 10^{-3}$
4	$9.7(2) \times 10^{-5}$	$1.25(2) \times 10^{-4}$	$1.06(2) \times 10^{-3}$	$1.30(2) \times 10^{-3}$
5	$6.1(2) \times 10^{-5}$	$8.6(2) \times 10^{-5}$	$8.7(1) \times 10^{-4}$	$1.08(1) \times 10^{-3}$
6	$4.9(2) \times 10^{-5}$	$7.1(2) \times 10^{-5}$	$7.3(1) \times 10^{-4}$	$9.2(1) \times 10^{-4}$
7	$4.2(2) \times 10^{-5}$	$6.2(1) \times 10^{-5}$	$6.1(1) \times 10^{-4}$	$7.6(1) \times 10^{-4}$
8	$3.8(2) \times 10^{-5}$	$5.5(1) \times 10^{-5}$	$4.9(1) \times 10^{-4}$	$6.08(9) \times 10^{-4}$
9	$3.4(2) \times 10^{-5}$	$5.0(1) \times 10^{-5}$	$3.7(1) \times 10^{-4}$	$4.53(7) \times 10^{-4}$
10	$3.1(2) \times 10^{-5}$	$4.6(1) \times 10^{-5}$	$2.5(1) \times 10^{-4}$	3.0251×10^{-4}
11	$2.9(2) \times 10^{-5}$	$4.3(1) \times 10^{-5}$	$1.2(1) \times 10^{-4}$	$1.49(3) \times 10^{-4}$
12	$2.8(2) \times 10^{-5}$	$4.2(1) \times 10^{-5}$	0	0

[1] A. Bazavov et al. (HotQCD Collaboration), Phys. Lett. B **795**, 15 (2019).
[2] H. T. Ding et al. (HotQCD Collaboration), Phys. Rev. Lett. **123**, 062002 (2019).
[3] E. V. Shuryak, Phys. Rev. D **42**, 1764 (1990).
[4] J. Goity and H. Leutwyler, Phys. Lett. B **228**, 517 (1989).
[5] J. Gasser and H. Leutwyler, Phys. Lett. B **188**, 477 (1987).
[6] P. Gerber and H. Leutwyler, Nucl. Phys. **B321**, 387 (1989).
[7] A. Schenk, Phys. Rev. D **47**, 5138 (1993).
[8] D. Toublan, Phys. Rev. D **56**, 5629 (1997).
[9] R. D. Pisarski and M. Tytgat, Phys. Rev. D **54**, R2989 (1996).
[10] D. T. Son and M. A. Stephanov, Phys. Rev. Lett. **88**, 202302 (2002).
[11] D. T. Son and M. A. Stephanov, Phys. Rev. D **66**, 076011 (2002).
[12] B. B. Brandt, A. Francis, H. B. Meyer, and D. Robaina, Phys. Rev. D **90**, 054509 (2014).
[13] B. B. Brandt, A. Francis, H. B. Meyer, and D. Robaina, Phys. Rev. D **92**, 094510 (2015).
[14] M. Lüscher, in Les Houches Summer School in Theoretical Physics, Session 68: Probing the Standard Model of Particle Interactions (North Holland, 1998), pp. 229–280, arXiv:hep-lat/9802029.
[15] H. B. Meyer, Eur. Phys. J. A **47**, 86 (2011).
[16] J. Bulava, M. Della Morte, J. Heitger, and C. Wittemeier (ALPHA Collaboration), Nucl. Phys. **B896**, 555 (2015).
[17] A. Gerardin, T. Harris, and H. B. Meyer, Phys. Rev. D **99**, 014519 (2019).
[18] I. Campos, P. Fritzsch, C. Pena, D. Preti, A. Ramos, and A. Vladikas (ALPHA Collaboration), Eur. Phys. J. C **78**, 387 (2018).
[19] J. Bulava and S. Schaefer, Nucl. Phys. **B874**, 188 (2013).
[20] M. Bruno et al., J. High Energy Phys. 02 (2015) 043.
[21] D. Mohler, S. Schaefer, and J. Simeth, EPJ Web Conf. **175**, 02010 (2018).
[22] M. Bruno, T. Korzec, and S. Schaefer, Phys. Rev. D **95**, 074504 (2017).
[23] M. Cè et al., Phys. Rev. D **106**, 114502 (2022).
[24] M. Lüscher and S. Schaefer, Comput. Phys. Commun. **184**, 519 (2013).
[25] W. Press, S. Teukolsky, W. Vetterling, and B. Flannery, Numerical Recipes: The Art of Scientific Computing (Cambridge University Press, Cambridge, England, 2007), 3rd ed.
[26] A. Bazavov et al., Phys. Rev. D **100**, 094510 (2019).
[27] M. Cè, A. Gérardin, G. von Hippel, H. B. Meyer, K. Miura, K. Ottnad, A. Risch, T. San José, J. Wilhelm, and H. Wittig, J. High Energy Phys. 08 (2022) 220.
[28] G. Backus and F. Gilbert, Geophys. J. Int. **16**, 169 (1968).
[29] D. Goderidze, A. Friesen, and Y. Kalinovsky, Int. J. Mod. Phys. A **37**, 2250135 (2022).
[30] S. Borsanyi, Z. Fodor, S. D. Katz, S. Krieg, C. Ratti, and K. Szabo, J. High Energy Phys. 01 (2012) 138.

[31] R. Hagedorn, Lect. Notes Phys. **221,** 53 (1985).
[32] F. Karsch, K. Redlich, and A. Tawfik, Eur. Phys. J. C **29,** 549 (2003).
[33] B. B. Brandt, A. Francis, B. Jäger, and H. B. Meyer, Phys. Rev. D **93,** 054510 (2016).
[34] M. Davier, A. Hocker, and Z. Zhang, Rev. Mod. Phys. **78,** 1043 (2006).
[35] R. Rapp and J. Wambach, Adv. Nucl. Phys. **25,** 1 (2000).
[36] J. I. Kapusta and E. V. Shuryak, Phys. Rev. D **49,** 4694 (1994).
[37] P. M. Hohler and R. Rapp, Phys. Lett. B **731,** 103 (2014).
[38] M. Dey, V. L. Eletsky, and B. L. Ioffe, Phys. Lett. B **252,** 620 (1990).
[39] V. L. Eletsky and B. L. Ioffe, Phys. Rev. D **47,** 3083 (1993).
[40] V. L. Eletsky and B. L. Ioffe, Phys. Rev. D **51,** 2371 (1995).
[41] H. B. Meyer, J. High Energy Phys. 04 (2010) 099.
[42] J. Gasser and H. Leutwyler, Phys. Lett. B **184,** 83 (1987).

[43] G. Aarts, C. Allton, D. De Boni, S. Hands, B. Jäger, C. Praki, and J.-I. Skullerud, J. High Energy Phys. 06 (2017) 034.
[44] M. Galassi *et al.*, GNU Scientific Library Reference Manual (3rd ed.), http://www.gnu.org/software/gsl/.
[45] L. Fousse, G. Hanrot, V. Lefèvre, P. Pélissier, and P. Zimmermann, ACM Trans. Math. Softw. **33,** 13–es (2007).
[46] T. Granlund (The GMP Development Team), The GNU Multiple Precision Arithmetic Library (2020), https://gmplib.org/.
[47] P. Korcyl and G. S. Bali, Phys. Rev. D **95,** 014505 (2017).
[48] M. Dalla Brida, T. Korzec, S. Sint, and P. Vilaseca, Eur. Phys. J. C **79,** 23 (2019).
[49] M. H. Quenouille, Biometrika **43,** 353 (1956).
[50] C. Gattringer and C. B. Lang, *Quantum Chromodynamics on the Lattice* (Springer, Berlin, 2010), Vol. 788.
[51] S. Bouma, G. Bali, S. Collins, and W. Söldner (RQCD Collaboration), Proc. Sci. LATTICE2021 (**2022**) 548 [arXiv:2206.04178].